A generalized approach for remaining useful life prediction considering the multi-source uncertainty of mechanical systems

OPEN ACCESS
IOP Publishing | ISECAEP
Journal of Reliability Science and Engineering
J. Reliab. Sci. Eng. **1** (2025) 025301 (14pp)
https://doi.org/10.1088/3050-2454/add5fa

A generalized approach for remaining useful life prediction considering the multi-source uncertainty of mechanical systems

Haoyan Gu[1], **Yong Li**[1,*], **Long Jiang**[2] and **Zhi Luo**[1]

[1] School of Mechanical and Power Engineering, East China University of Science and Technology, Shanghai, People's Republic of China
[2] State Key Laboratory of Oil and Gas Equipment, CNPC Tubular Goods Research Institute, Xi'an, People's Republic of China

E-mail: liyong@ecust.edu.cn

Received 17 January 2025, revised 18 March 2025
Accepted for publication 22 April 2025
Published 21 May 2025

Abstract

Mechanical system remaining useful life (RUL) prediction accuracy is often influenced by uncertain factors such as individual differences, degradation volatility, and failure threshold (FT) randomness. Current age- and state-dependent Wiener process models (WPMs) are implemented by considering only the constant diffusion coefficient and fixed FT, which are difficult to apply in practical engineering. To address this problem, a generalized approach is proposed for RUL prediction by considering the multi-source uncertainty of mechanical systems. In this approach, an improved age- and state-dependent WPM is proposed by introducing a unit-to-unit variability-included diffusion coefficient, and the model parameters are estimated by a modified artificial bee colony algorithm-based maximum likelihood estimation. After that, the two unit-to-unit variability parameters are synchronously updated by using an adaptive Kalman filter. And then, the probability density function of RUL is approximated by the degradation process simulation method under the condition that the random FT follows a truncated normal distribution. The effectiveness of the proposed method is verified experimentally, and the results show better prediction accuracy than commonly used models, which offers an alternative solution for RUL prediction of mechanical systems.

Keywords: Wiener process model, remaining useful life prediction, multi-parameter optimization, random failure threshold

* Author to whom any correspondence should be addressed.

1. Introduction

Remaining useful life (RUL) prediction is a significant component of prognostics and health management (PHM) [1–3]. Currently, two types of methods, physical model-based and data-driven, are often used for RUL prediction. The physical model is developed based on the failure mechanism, which allows for a precise description of a machine's degradation process [4, 5]. Although physical model-based methods can effectively predict the RUL, with an increase in mechanical complexity, obtaining an accurate physical model becomes increasingly difficult and time-consuming. Owing to the development of Internet of Things technology, data-driven methods have received increasing attention in recent years [6]. Data-driven methods can be broadly classified into two types: stochastic process- and machine learning-based methods. Machine learning can predict RUL by autonomously learning the mapping relationship between condition monitoring (CM) data and failure time. With the acquisition of big data, relevant techniques have been widely applied to RUL prediction, and both the accuracy and uncertainty have been discussed. For example, Peng *et al* [7] developed a Bayesian deep-learning-based method to quantify uncertainty. Chen *et al* [8] designed a prediction interval and used a bidirectional long short-term memory network to obtain the distribution interval of RUL. To quantify the prediction uncertainty. Liu *et al* [9] proposed a novel loss function that allows the deep learning model to output the prediction variance. However, the obtained uncertainties heavily depend on the designed regularization techniques [10]. Since machine-learning-based methods primarily focus on minimizing the prediction error, which makes it challenging to fully capture the multi-source uncertainty inherent in the degradation process. By contrast, stochastic process models have a natural advantage in quantifying uncertainty.

In the field of RUL prediction, the Wiener process model (WPM) is one of the most widely used models due to its great physical interpretability and mathematical characteristics [11]. In general, the WPM consists of a drift term and a diffusion term, which reflect the degradation trend and volatility, respectively. WPM-based methods predict RUL by fitting the degradation pattern of the health state and extrapolating it to the failure threshold (FT). Therefore, it is important to accurately describe the actual degradation process for prediction accuracy. Traditional WPMs are age-dependent, which have good computational properties and have been well studied. For example, Liu *et al* [12] replaced the drift function with an artificial neural network to improve the fitting effect. Yang *et al* [13] considered both individual difference and measurement error to improve the prediction accuracy. Zhang *et al* [14] introduced a dynamic covariate to describe the dynamic and stochastic operating conditions.

However, age-dependent models can provide precise RUL prediction results when the degradation process is driven only by time. In fact, practical degradation processes are often influenced by both the system's age and current state, which has been demonstrated in various materials [15–17]. Zhang *et al* [18] first studied the application of an age- and state-dependent WPM in RUL prediction. Based on this model, Li *et al* [19, 20] developed model update and RUL probability density function (PDF) calculation methods to improve prediction accuracy. Pang *et al* [21] quantifies and estimates the uncertainty caused by measurement errors. Zhai *et al* [22] constructed a two-scale WPM of age and usage, which fits better than the single-scale model. He *et al* [23] replaced the explicit drift coefficient with a neural network to better capture the degradation features from CM data. In the above models, the diffusion coefficient is simplified to a constant. In practice, the stability of a mechanical system usually decreases with degradation development, which not only leads to an increase in the degradation rate, but also increases the degradation volatility. However, the constant diffusion coefficient cannot describe the dynamic characteristics of the volatility. From the perspective of the correlation between the volatility and rate, Ye *et al* [24] established a diffusion coefficient that was positively correlated with the degradation rate, and verified the superiority of the model using fatigue crack propagation data. Wang *et al* [25] established a quantitative relationship between the drift and diffusion coefficients, but the rigorous proof applies only to the basic Wiener process. Wang *et al* [26] further proposed a revised scaling relation suitable for the drift term of power functions. Considering the time-varying feature of the volatility, Zhang *et al* [27] proposed a diffusion term with history dependence. Ge *et al* [28] added a thick-tailed distribution term to describe the additive errors in the true degradation path. Zhou *et al* [29] further considered the rate dependence and time variability of the volatility simultaneously. Nevertheless, due to differences in manufacturing and assembly processes, monitoring equipment and working environment, volatility can also vary among different individuals [30, 31]. Current studies neglect this factor and are mostly based on traditional WPMs, which, as discussed earlier, have limited fitting capability.

Moreover, it is important to note that these prediction methods discussed above ignore random FT (RFT). Due to various uncertainties in both the degradation and monitoring process of a mechanical system, it is difficult to determine a precise FT [32, 33]. Therefore, the RFT is a critical factor that must be considered in practice. Tang *et al* [34] used the linear degradation model to deduce the RUL PDF under the truncated normal distribution by considering the non-negativity of FT. On this basis, Wang *et al* [35] derived the RUL PDF formula based on the nonlinear WPM. Wang *et al* [36] constructed a RFT based on the degradation model to reduce the observation error. Although researchers have considered the RFT in RUL prediction, most of these only studies the age-dependent degradation processes.

As discussed above, although current age- and state-dependent WPM-based methods have shown different levels of success in RUL prediction, these models are implemented by only considering the constant diffusion coefficient, or ignoring the uncertainty effects of the FT, which severely limits their practical applications. To address these problems, a systematic framework is established in this study for the RUL

prediction of rotary machinery systems, and the main contributions are as follows.

(1) To enhance the practicality of the model, an improved age- and state-dependent WPM is proposed by introducing a novel time-varying diffusion coefficient which contains a unit-to-unit variability parameter.
(2) To address the shortcomings of existing methods, a maximum likelihood estimation (MLE) based on an improved artificial bee colony (IABC) algorithm is proposed for multi-parameter estimation. Subsequently, an adaptive Kalman filter (AKF) is introduced to update both unit-to-unit variability parameters without assuming a predefined quantitative relationship between them.
(3) The RFT is introduced in the proposed method, and the closed-form solution of the RUL PDF is derived and approximately calculated under the RFT that follows a truncated normal distribution.

The rest of this paper is organized as follows. After a brief introduction to the age- and state-dependent WPM, the general expression of the improved model is proposed in section 2. Section 3 introduces the processes of parameter estimation, parameter updating and RUL estimation under the RFT that follows a truncated normal distribution. In section 4, the performance of the proposed model is evaluated by using two experimental datasets. Finally, concluding remarks are presented in section 5.

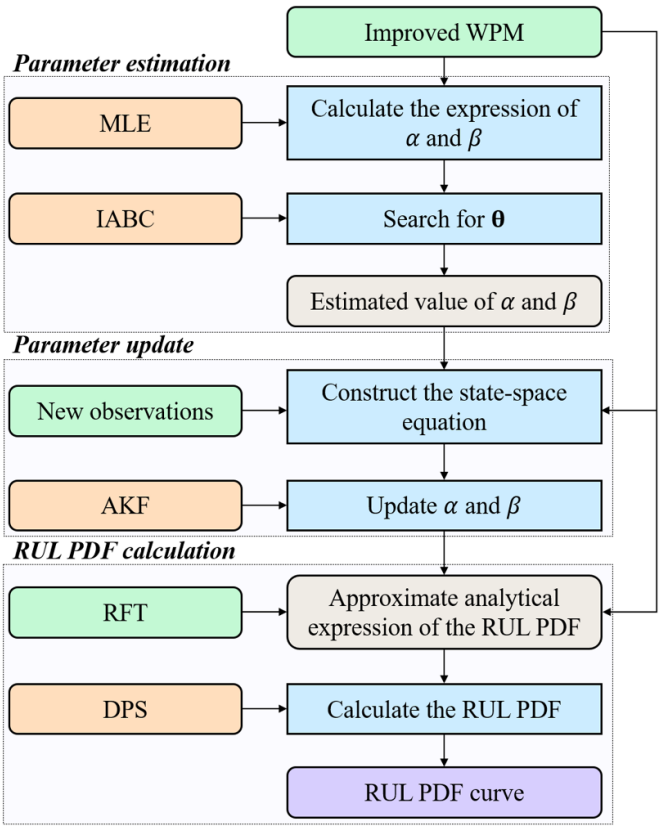

Figure 1. Process of the proposed RUL prediction method.

2. Degradation model

Let $\{x(t), t \geqslant t_m\}$ represent the degradation process of a stochastic system. By using the framework of the age- and state-dependent WPM, the general expression of $\{x(t), t \geqslant t_m\}$ can be expressed as follows:

$$x(t) = x_m + \int_{t_m}^{t} \mu(x(\tau), \tau)\,\mathrm{d}\tau + \int_{t_m}^{t} \sigma(\tau)\,\mathrm{d}B(\tau), \quad (1)$$

where $x(t)$ is the state at time t, with $t \geqslant t_m$, t_m is the initial time of the degradation process, and x_m is the state at time t_m; $\mu(x(\tau), \tau)$ is the coefficient function of the drift term, which may depend on the age and state of the system; $\sigma(\tau)$ is the diffusion coefficient; $B(\tau)$ is a standard Brownian motion (BM) process.

Current age- and state-dependent WPMs consider the diffusion coefficient to be constant, which may constrain their practical applications. Although an adaptive diffusion coefficient was revealed by Wang *et al* [37], the proposed quantitative relationship between the diffusion coefficient and drift coefficient is limited by the basic age-dependent WPM and some specific assumptions. To overcome this constraint, this study introduces an additional unit-to-unit variability parameter into the diffusion term, and the improved age- and state-dependent WPM is proposed as follows:

$$x(t) = x_m + \alpha \int_{t_m}^{t} \Lambda(x(\tau), \tau; \boldsymbol{\theta})\mathrm{d}\tau + \beta \int_{t_m}^{t} \sigma(\tau; \boldsymbol{\theta})\,\mathrm{d}B(\tau), \quad (2)$$

where $\Lambda(x(\tau), \tau; \boldsymbol{\theta})$ and $\sigma(\tau; \boldsymbol{\theta})$ are the drift and diffusion coefficient functions, respectively; α and β are the unit-to-unit variability parameters, which are used to reflect the differences between individuals; $\boldsymbol{\theta}$ is the parameter vector composed of fixed parameters, which can reflect the consistent degradation features among the same systems.

2.1. RUL prediction

For practical applications, the proposed model should be implemented in the following three steps. First, historical degradation data must be employed in this model for unknown parameter estimation. Then, new observations from the on-site system are required to update the model parameters. Finally, the RUL PDF is calculated by using the adjusted model in step two. Figure 1 shows a flowchart of the proposed method, and the detailed process is elaborated upon in the following sections.

2.2. Parameter estimation

Degradation models are often discussed in the continuous time domain. However, the degradation monitoring process of a mechanical system is described in the discrete time domain. Thus, the proposed model given by equation (2) should be discretized before parameter estimation. Suppose that there are N training specimens $\{\boldsymbol{x}_n\}_{n=1}^{N}$, and $\boldsymbol{x}_n = [x_{n,1},\cdots,x_{n,m},\cdots,x_{n,M_n}]^{\mathrm{T}}$ are the state observation values of the n th specimen at time $t_{n,1},\cdots,t_{n,m},\cdots,t_{n,M_n}$, where M_n is the number of observations in the n th specimen. Since the drift term of the degradation model may be related to the state, the Euler discretization method [38] is introduced to approximate the degradation model in this study.

After discretizing, the state degradation amount $\Delta x_{n,m}$ can be expressed as

$$\Delta x_{n,m} = \alpha_n \Lambda\left(x_{n,m}, t_{n,m}; \boldsymbol{\theta}\right) \Delta t_{n,m} + \zeta_{n,m}, \tag{3}$$

where $\Delta t_{n,m} = t_{n,m+1} - t_{n,m}$ is the time interval between two adjacent observations, $\zeta_{n,m} \sim N\left(0, \beta_n^2 \kappa_{n,m}^2\right)$, with $\kappa_{n,m}^2 = \int_{t_{n,m}}^{t_{n,m+1}} \sigma^2\left(\tau;\boldsymbol{\theta}\right) \mathrm{d}\tau$.

Let $\Delta\boldsymbol{x}_n = [x_{n,2} - x_{n,1}, \cdots x_{n,M_n} - x_{n,M_n-1}]^{\mathrm{T}}$. According to the property of the Wiener process [39], $\Delta\boldsymbol{x}_n$ follows a multivariate normal distribution $N\left(\alpha_n \boldsymbol{T}_n, \beta_n^2 \boldsymbol{\Omega}_n\right)$, with

$$\boldsymbol{T}_n = [\mathrm{T}_{n,1},\cdots,\mathrm{T}_{n,m},\cdots,\mathrm{T}_{n,M_n-1}]^{\mathrm{T}}, \tag{4}$$

$$\boldsymbol{\Omega}_n = \mathrm{diag}\left(\left[\kappa_{n,1}^2,\cdots,\kappa_{n,m}^2,\ldots,\kappa_{n,M_n-1}^2\right]\right), \tag{5}$$

where $\mathrm{T}_{n,m} = \Lambda\left(x_{n,m}, t_{n,m};\boldsymbol{\theta}\right)\Delta t_{n,m}$, $\boldsymbol{\Omega}_n$ denotes a $M_n - 1$ dimensional diagonal matrix, and its main diagonal is $[\kappa_{n,1}^2, \kappa_{n,2}^2, \ldots, \kappa_{n,M_n-1}^2]$.

The unknown parameters $\left\{\alpha_1,\ldots,\alpha_N,\beta_1^2,\ldots,\beta_N^2,\boldsymbol{\theta}\right\}$ are estimated by using the historical data. Let $x = \{\Delta\boldsymbol{x}_1, \Delta\boldsymbol{x}_2, \ldots, \Delta\boldsymbol{x}_N\}$ represent the degradation data of all training specimens, then the log-likelihood function of x can be expressed as

$$\begin{aligned} l(\varkappa) = &-\frac{\ln(2\pi)}{2}\sum_{n=1}^{N}(M_n-1) - \frac{1}{2}\sum_{n=1}^{N}(M_n-1)\ln\left(\beta_n^2\right) \\ &-\frac{1}{2}\sum_{n=1}^{N}\ln|\boldsymbol{\Omega}_n| \\ &-\frac{1}{2}\sum_{n=1}^{N}\frac{\left(\Delta\boldsymbol{x}_n - \alpha_n\boldsymbol{T}_n\right)^{\mathrm{T}}\boldsymbol{\Omega}_n^{-1}\left(\Delta\boldsymbol{x}_n - \alpha_n\boldsymbol{T}_n\right)}{\beta_n^2}. \end{aligned} \tag{6}$$

Let the first-order partial derivatives of equation (6) with respect to α_n and β_n equal to 0. The estimation results can be calculated as

$$\hat{\alpha}_n = \frac{{\boldsymbol{T}_n}^{\mathrm{T}}\boldsymbol{\Omega}_n^{-1}\Delta\boldsymbol{x}_n}{{\boldsymbol{T}_n}^{\mathrm{T}}\boldsymbol{\Omega}_n^{-1}\boldsymbol{T}_n}, \tag{7}$$

$$\hat{\beta}_n^2 = \frac{\left(\Delta\boldsymbol{x}_n - \alpha_n\boldsymbol{T}_n\right)^{\mathrm{T}}\boldsymbol{\Omega}_n^{-1}\left(\Delta\boldsymbol{x}_n - \alpha_n\boldsymbol{T}_n\right)}{M_n - 1}. \tag{8}$$

Substituting equations (7) and (8) into equation (6), it is found that the log-likelihood function equation (6) is related only to $\boldsymbol{\theta}$. Since solving the expressions for other parameters, especially those in nonlinear terms, is difficult, derivative-free optimization algorithms are usually utilized to solve this problem, such as the Nelder–Mead algorithm [40]. However, this method is often used for unconstrained problems and for simple models. Because of its sensitivity to initial conditions and inefficiency in high-dimensional spaces [41], it is impractical for complicated nonlinear models with multiple parameters. In addition, potential constraints on the parameters may result from considering the effects of multiple influencing factors. For example, the growth rate of a fatigue crack should be positively correlated with its current length [42], which means that the coefficient of the state term should be nonnegative. Therefore, this study introduces an artificial bee colony (ABC) algorithm [43] to search $\boldsymbol{\theta}$, which is further improved for this problem. The specific estimation process is as follows.

Firstly, a series of solutions $\left\{\boldsymbol{\theta}_n^0\right\}_{n=1}^{Nt}$ is generated randomly from an initial search space, where Nt is the number of solutions. It should be noted that this space is not strongly confined, and the search capability can be artificially controlled. The generation rule is

$$\theta_{n,d}^0 = L_d + o\left(U_d - L_d\right), \tag{9}$$

where $d = 1,\ 2,\cdots,D$, and D is the number of unknown parameters; o is a random variable drawn from the uniform distribution $U(0,1)$; U_d and L_d are the upper and lower bounds of the search space.

The search mechanism has a significant impact on the performance of the algorithm. To accelerate the convergence speed, the standard search mechanism can be improved [44, 45], such as

$$\theta_{n,s}'^{i} = \begin{cases} \theta_{n,s}^{i-1} + \rho_{n,s}\cdot\left(\theta_{n,s}^{i-1} - \theta_{\mathrm{best},s}^{i-1}\right), & p < SP \\ \theta_{n,s}^{i-1} + \phi_{n,s}\cdot\left(\theta_{n,s}^{i-1} - \theta_{r,s}^{i-1}\right), & p \geqslant SP \end{cases}, \tag{10}$$

where s is an index that specifies the parameter that needs to be searched in the i th iteration; θ_{best} is the optimal solution; $p \sim U(0,1)$; SP is the selection probability; $r \in \{1,\ 2,\cdots,Nt\}$, and $r \neq n$; $\rho \sim U(-u,0)$ and $\phi \sim U(-u,u)$, where u is the disturbance amplitude.

In general, a specified number of parameters are randomly selected to update each time. From equation (6), it can be observed that the maximum value of the normal distribution PDF is mainly determined by the error between the actual observations and average estimation results, that is, it is related to the parameters in the drift term. This implies that search complexity may be different for each parameter. For example, a good estimate of α_n can be obtained by minimizing the gap

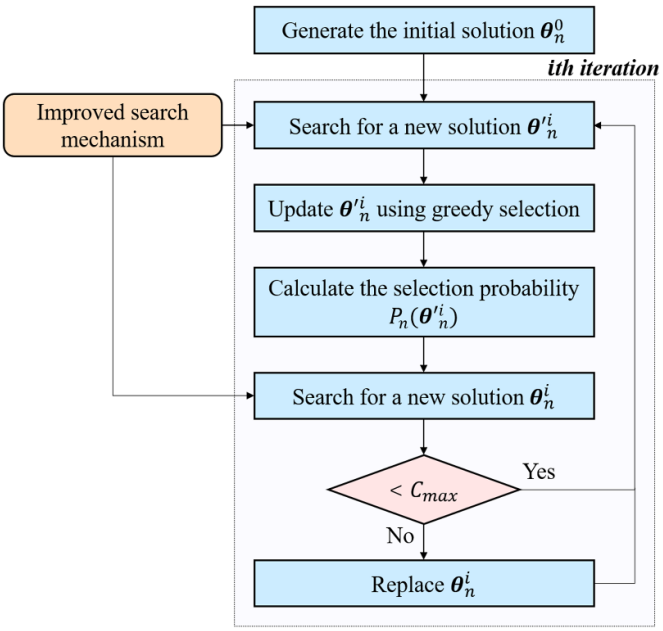

Figure 2. Process of the IABC algorithm.

between $\Delta \boldsymbol{x}_n$ and $\alpha_n \boldsymbol{T}_n$, which is less influenced by the parameters in the diffusion term. Furthermore, some parameters may also require more iterations to be adjusted by considering the error between the initial search space and optimal results. Therefore, the improved method pays attention to the change of parameters to set the appropriate selection probability, which is

$$P_d = \begin{cases} \frac{1}{D},\ i = 1,3,5,\ldots \\ \frac{\left|\left(\theta^i_{\text{best},d} - \theta^{i-1}_{\text{best},d}\right)/\theta^{i-1}_{\text{best},d}\right|}{\sum_{d=1}^{D}\left|\left(\theta^i_{\text{best},d} - \theta^{i-1}_{\text{best},d}\right)/\theta^{i-1}_{\text{best},d}\right|},\ i = 2,4,6,\ldots \end{cases}, \tag{11}$$

The specific iterative process of the algorithm is shown in figure 2 and the details are described below.

(1) Search new solutions $\left\{\boldsymbol{\theta}_n^{\prime i}\right\}_{n=1}^{Nt}$ around $\left\{\boldsymbol{\theta}_n^{i-1}\right\}_{n=1}^{Nt}$ according to equation (10).

(2) Determine the solutions needed to be retained according to the greedy selection method, and update $\boldsymbol{\theta}_n^{\prime i}$ as

$$\boldsymbol{\theta}_n^{\prime i} = \begin{cases} \boldsymbol{\theta}_n^{i-1},\ l\left(\boldsymbol{\theta}_n^{\prime i}\right) < l\left(\boldsymbol{\theta}_n^{i-1}\right) \\ \boldsymbol{\theta}_n^{\prime i}, l\left(\boldsymbol{\theta}_n^{\prime i}\right) \geqslant l\left(\boldsymbol{\theta}_n^{i-1}\right) \end{cases}. \tag{12}$$

(3) Calculate the selection probability of each solution based on its fitness. The fitness and selection probability of $\boldsymbol{\theta}_n^{\prime i}$ are computed as follows

$$F_n\left(\boldsymbol{\theta}_n^{\prime i}\right) = \exp\left(\frac{l\left(\boldsymbol{\theta}_n^{\prime i}\right)}{\sum_{n=1}^{Nt}\left|l\left(\boldsymbol{\theta}_n^{\prime i}\right)\right|}\right), \tag{13}$$

$$P_n\left(\boldsymbol{\theta}_n^{\prime i}\right) = \frac{F_n\left(\boldsymbol{\theta}_n^{\prime i}\right)}{\sum_{n=1}^{Nt} F_n\left(\boldsymbol{\theta}_n^{\prime i}\right)}. \tag{14}$$

(4) Based on the selection probabilities, Nt solutions $\left\{\boldsymbol{\theta}_n^{*i}\right\}_{n=1}^{Nt}$ are selected from $\left\{\boldsymbol{\theta}_n^{\prime i}\right\}_{n=1}^{Nt}$ using the roulette wheel method. Subsequently, the final solutions $\left\{\boldsymbol{\theta}_n^{i}\right\}_{n=1}^{Nt}$ of the i th iteration are generated from $\left\{\boldsymbol{\theta}_n^{*i}\right\}_{n=1}^{Nt}$ according to equation (10).

(5) If the solution is not updated in $C_{\max}$ iterations, a new solution is regenerated according to equation (9) to replace the original one.

The best solution $\boldsymbol{\theta}^i_{\text{best}}$ is selected as the optimal solution $\widehat{\theta}^i$. Then, steps 1)-5) are repeated until $\|\widehat{\boldsymbol{\theta}}^i - \widehat{\boldsymbol{\theta}}^{i-1}\|$ is less than the preset threshold.

2.2.1. Parameter update. Since the degradation process differs among individuals, the unit-to-unit variability parameters of the online system must be updated by using its actual degradation data. In known models, unit-to-unit variability only appears in the degradation trend, and as a result, commonly used methods have been developed to update the unit-to-unit variability parameter in the drift term [20, 21, 46]. However, in the proposed model, the unit-to-unit variability parameter β in the diffusion term must also be updated. Here, an AKF based on the MLE is introduced to synchronously update the parameter α and β. The state-space equation can be expressed as

$$\begin{cases} \alpha_k = \alpha_{k-1} \\ \Delta x_k = \mathrm{T}_k \alpha_k + R_k \end{cases}, \tag{15}$$

where $\Delta x_k = x_{k+1} - x_k$ is state degradation value of the online system from time t_k to t_{k+1}; $\mathrm{T}_k = \Lambda\left(x_k,\ t_k; \boldsymbol{\theta}\right)\left(t_{k+1} - t_k\right)$; $R_k \sim N\left(0, \beta_k^2 \kappa_k^2\right)$ and $\kappa_k^2 = \int_{t_k}^{t_{k+1}} \sigma^2\left(\tau; \boldsymbol{\theta}\right) \mathrm{d}\tau$.

Referring to the ensemble Kalman filter [47], the particles $\{\hat{\alpha}_n\}_{n=1}^{N}$ obtained in the parameter estimation are used to approximate the PDF of α. The parameter estimation results $\{\hat{\alpha}_n\}_{n=1}^{N}$ and $\left\{\hat{\beta}_n^2\right\}_{n=1}^{N}$ are taken as the initial particles and denoted by $\{\alpha_{n,0}\}_{n=1}^{N}$ and $\{\beta_{n,0}\}_{n=1}^{N}$, respectively. According to the principle of Kalman filter, the updated $\{\alpha_{n,k}\}_{n=1}^{N}$ after the k th iteration can be expressed as

$$\alpha_{n,k} = \alpha_{n,k}^f + K_{n,k}\left(\Delta x_k - \mathrm{T}_k \alpha_{n,k}^f + R_{n,k}\right), \tag{16}$$

with

$$K_{n,k} = P_k^f H_k^{\mathrm{T}}\left(H_k P_k^f H_k^{\mathrm{T}} + \beta_{n,k}^2 \kappa_k^2\right)^{-1}, \tag{17}$$

$$P_k^f H_k^{\mathrm{T}} = \frac{1}{N-1}\sum_{n=1}^{N}\left(\alpha_{n,k}^f - \bar{\alpha}_k^f\right)\left(\mathrm{T}_k\alpha_{n,k}^f - \mathrm{T}_k\bar{\alpha}_k^f\right), \quad (18)$$

$$H_k P_k^f H_k^{\mathrm{T}} = \frac{1}{N-1}\sum_{n=1}^{N}\left(\mathrm{T}_k\alpha_{n,k}^f - \mathrm{T}_k\bar{\alpha}_k^f\right)^2, \quad (19)$$

where $\alpha_{n,k}^f = \alpha_{n,k-1}$ is the predicted value of $\alpha_{n,k}$; $\bar{\alpha}_k^f = \sum_{n=1}^{N}\left(\alpha_{n,k}^f\right)/N$; $R_{n,k} \sim N\left(0, \beta_{n,k}^2\kappa_k^2\right)$.

Subsequently, $\left\{\beta_{n,k}^2\right\}_{n=1}^{N}$ can be updated by using MLE. Suppose that the error sequence $\boldsymbol{v}_{n,k}$ between the observations and the updated results follows a multivariate normal distribution $N(0, \boldsymbol{\upsilon}_{n,k})$, where

$$\boldsymbol{v}_{n,k} = \left[\Delta x_1 - \mathrm{T}_1\alpha_{n,1}, \ldots, \Delta x_k - \mathrm{T}_k\alpha_{n,k}\right]^{\mathrm{T}}, \quad (20)$$

$$\boldsymbol{\upsilon}_{n,k} = \mathrm{diag}\left(\left[\beta_{n,1}^2\kappa_1^2, \beta_{n,2}^2\kappa_2^2, \ldots, \beta_{n,k}^2\kappa_k^2\right]\right). \quad (21)$$

The log-likelihood function of $\boldsymbol{v}_{n,k}$ can be expressed as

$$l\left(\beta_{n,k}^2|\boldsymbol{v}_{n,k}\right) = -\frac{k}{2}\ln(2\pi) - \frac{1}{2}\ln|\boldsymbol{\upsilon}_{n,k}| - \frac{1}{2}\boldsymbol{v}_{n,k}^{\mathrm{T}}\boldsymbol{\upsilon}_{n,k}^{-1}\boldsymbol{v}_{n,k}. \quad (22)$$

Then, $\left\{\beta_{n,k}^2\right\}_{n=1}^{N}$ can be obtained by maximizing equation (22). By ignoring the constant terms, the MLE problem becomes

$$\beta_{n,k}^2 = \mathrm{argmin}\left[\ln|\boldsymbol{\upsilon}_{n,k}| + \boldsymbol{v}_{n,k}^{\mathrm{T}}\boldsymbol{\upsilon}_{n,k}^{-1}\boldsymbol{v}_{n,k}\right]. \quad (23)$$

Considering the potential instability at the early stage of degradation, a window of size W is used for data filtering. Based on the principle of adaptive Kalman filter [48], $\beta_{n,k}^2$ can be computed as

$$\beta_{n,k}^2 = \frac{\sum_{i=i_0}^{k} H_i P_i H_i^{\mathrm{T}} + \sum_{i=i_0}^{k}\left(\Delta x_i - \mathrm{T}_i\alpha_{n,i}\right)^2}{\sum_{i=i_0}^{k}\kappa_i^2}, \quad (24)$$

where $i_0 = k - W + 1$ is the starting index;

$$H_i P_i H_i^{\mathrm{T}} = \frac{1}{N-1}\sum_{n=1}^{N}\left(\mathrm{T}_i\alpha_{n,i} - \mathrm{T}_i\bar{\alpha}_i\right)^2 \quad (25)$$

and $\bar{\alpha}_k = \sum_{n=1}^{N}\left(\alpha_{n,k}\right)/N$.

The median value $\bar{\alpha}_k$ and $\bar{\beta}_k^2$ of $\left\{\left[\alpha_{n,k}, \beta_{n,k}^2\right]\right\}_{n=1}^{N}$ after the k th iteration are used as the final update results. Once a new observation appears, new unit-to-unit variability parameters are generated by using the proposed method. Thus, the model can more accurately reflect the current degradation trend of the online machine.

2.2.2. RUL PDF calculation. The RUL of a mechanical system is defined as the time when the state degradation first exceeds the FT, which is called the first hit time (FHT). According to the definition of FHT, the RUL at t_m is expressed as

$$l_m = \inf\left\{l : x\left(t_m + l\right) \geqslant \lambda | x_m < \lambda\right\}, \quad (26)$$

where $\inf\{\cdot\}$ represents the lower bound of a variable; l_m is the RUL at time t_m; λ is the FT.

Since the system degradation is a random process, the RUL l_m is not a definite value. Lemma 1 provides the RUL PDF of the degradation process $\left\{x(t), t \geqslant t_m\right\}$ under a fixed FT λ [18].

Lemma 1: for the degradation process $\left\{x(t), t \geqslant t_m\right\}$ shown in equation (2), the RUL PDF under the conditions of initial time t_m and FT λ can be expressed as

$$f(l|x_m, \lambda) \cong \frac{1}{\sqrt{2\pi\,\psi(l)}}\left(\frac{\varphi(\lambda, l)}{\psi(l)} - \frac{\mathrm{d}\varphi(\lambda, l)}{\mathrm{d}\psi(l)}\right) \cdot \exp\left(-\frac{\varphi^2(\lambda, l)}{2\psi(l)}\right)\frac{\mathrm{d}\psi(l)}{\mathrm{d}l}, \quad (27)$$

where $\varphi(\lambda, l) = \lambda - x_m - \alpha\int_0^l \Lambda\left(x(\tau + t_m), \tau + t_m; \boldsymbol{\theta}\right)\mathrm{d}\tau$ and $\psi(l) = \beta^2\int_0^l \sigma^2\left(\tau + t_m; \boldsymbol{\theta}\right)\mathrm{d}\tau$.

In practical applications, due to the decrease in the stability of the degradation process and the influence of other uncertain factors, the observations at the point of failure vary among different systems. To address this, it is more appropriate to consider the FT as a random variable [49].

Assume that λ follows a truncated normal distribution $TN\left(\mu_\lambda, \sigma_\lambda^2\right)$, and the probability $\lambda < 0$ is truncated. To derive the RUL PDF for the RFT, Lemma 2 is given below [35].

Lemma 2: if $D \sim TN\left(\mu, \sigma^2\right)$. $F, G \in R, H \in R^+$, it exists

$$E_D\left[(D-F)\exp\left(-\frac{(D-G)^2}{2H}\right)\right] = \frac{1}{\sqrt{2\pi}\,\sigma\Phi(\mu/\sigma)}\exp\left(-\frac{(\mu-G)^2}{2(H+\sigma^2)}\right) \times\left[\frac{H\sigma^2}{H+\sigma^2}\exp\left(-\frac{\left(G\sigma^2+H\mu\right)^2}{2(H+\sigma^2)H\sigma^2}\right) + \sqrt{\frac{2\pi H\sigma^2}{H+\sigma^2}} \cdot\left(\frac{G\sigma^2+H\mu}{H+\sigma^2} - F\right)\Phi\left(\frac{G\sigma^2+H\mu}{\sqrt{(H+\sigma^2)H\sigma^2}}\right)\right]. \quad (28)$$

By combining Lemma 1 with Lemma 2, when $\lambda \sim TN\left(\mu_\lambda, \sigma_\lambda^2\right)$, the RUL PDF of the proposed model (as shown in equation (2)) can be expressed as

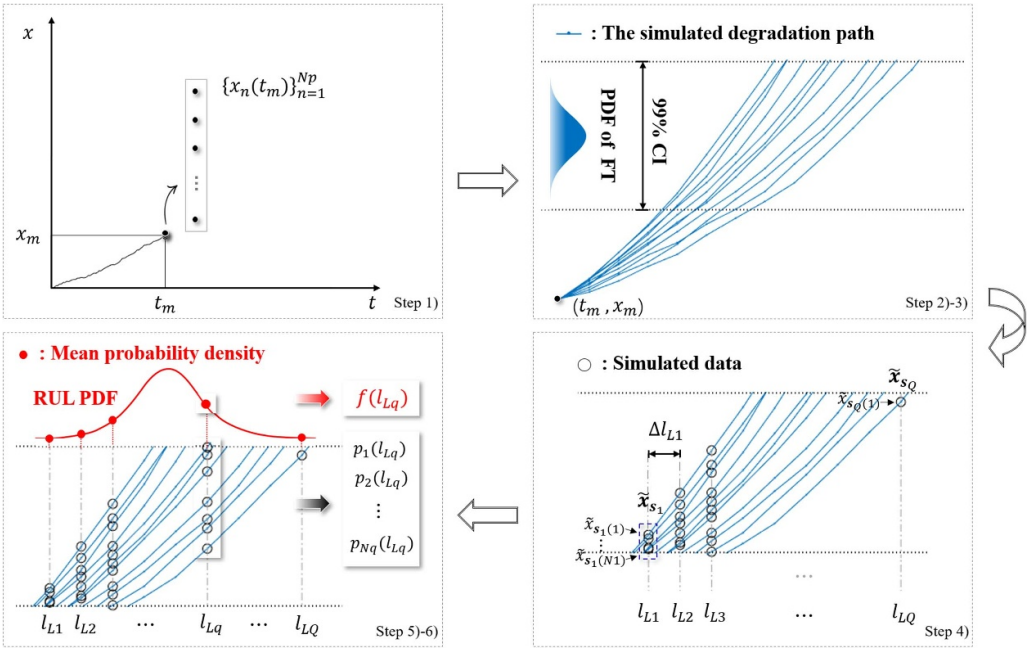

Figure 3. Procedure of the degradation process simulation.

$$f(l|x_m) = \frac{\beta^2\sigma^2(l+t_m;\boldsymbol{\theta})}{2\pi H\sqrt{H}\sigma_\lambda \Phi(\mu_\lambda/\sigma_\lambda)} \exp\left(-\frac{(\mu_\lambda - G)^2}{2(H+\sigma_\lambda^2)}\right) \times \left[\frac{H\sigma_\lambda^2}{H+\sigma_\lambda^2}\exp\left(-\frac{(G\sigma_\lambda^2+H\mu_\lambda)^2}{2(H+\sigma_\lambda^2)H\sigma_\lambda^2}\right) + \sqrt{\frac{2\pi H\sigma_\lambda^2}{H+\sigma_\lambda^2}} \cdot \left(\frac{G\sigma_\lambda^2+H\mu_\lambda}{H+\sigma_\lambda^2} - F\right)\Phi\left(\frac{G\sigma_\lambda^2+H\mu_\lambda}{\sqrt{(H+\sigma_\lambda^2)H\sigma_\lambda^2}}\right)\right], \tag{29}$$

where

$$F = G - H\frac{\alpha\Lambda(x(l+t_m), l+t_m;\boldsymbol{\theta})}{\beta^2\sigma^2(l+t_m;\boldsymbol{\theta})}, \tag{30}$$

$$G = x_m + \alpha\int_0^l \Lambda(x(\tau+t_m), \tau+t_m;\boldsymbol{\theta})\,\mathrm{d}\tau, \tag{31}$$

$$H = \beta^2\int_0^l \sigma^2(\tau+t_m;\boldsymbol{\theta})\,\mathrm{d}\tau. \tag{32}$$

Since the state-dependent term is contained in equation (29), it is difficult to calculate the RUL PDF directly using the analytical formula. To solve this problem, the DPS method is introduced for approximate processing [19]. The procedure of DPS is shown in figure 3. The specific steps are as follows.

(1) At the initial time t_m, Np simulation paths $\{x_n(t_m)\}_{n=1}^{Np}$ with the initial time t_m and state x_m are generated.

(2) The simulated data for each path are generated with the actual observation interval as

$$x_n(t_m+l_{i+1}) = x_n(t_m+l_i) + \alpha_n\Lambda(x_n(t_m+l_i), t_m+l_i;\boldsymbol{\theta})\Delta l_i + \xi_i, \tag{33}$$

where $x_n(t_m+l_i)$ is the state of the n th simulation path at time t_m+l_i $\left(i\in N^+,\ l_i=\sum_{j=1}^{i}\Delta l_j\right)$; Δl_i is the observation interval; $\xi_i \sim U(-3\varepsilon_i, 3\varepsilon_i)$ is a random noise, with $\varepsilon_i = \mathrm{sqrt}\left(\beta_n^2\int_{l_i}^{l_{i+1}}\sigma^2(t_m+\tau;\boldsymbol{\theta})\,\mathrm{d}\tau\right)$.

(3) The 99% confidence interval (CI) of the FT is used as the failure interval. Subsequently, step 2) is repeated until the simulation path exceeds the upper bound of the failure interval.

(4) The simulated data $\{\tilde{\boldsymbol{x}}_{\boldsymbol{s}_1},\ldots,\tilde{\boldsymbol{x}}_{\boldsymbol{s}_q},\ldots,\tilde{\boldsymbol{x}}_{\boldsymbol{s}_Q}\}$ in the failure interval are marked, where Q is the number of RULs that can be observed in the failure interval; $\tilde{\boldsymbol{x}}_{\boldsymbol{s}_q} = \{\tilde{x}_{s_q(1)},\ldots,\tilde{x}_{s_q(n)},\ldots,\tilde{x}_{s_q(Nq)}\}$ denote the simulated data at RUL l_{Lq}, and $\boldsymbol{s}_q$ is an index vector indicating the path to which the data belongs; Nq is the number of the data at l_{Lq}.

(5) The probability density $p_n(l=l_{Lq})$ of l_{Lq} corresponding to $\tilde{x}_{s_q(n)}$ is calculated by substituting $\tilde{x}_{s_q(n)}$ into equation (29), and the state-dependent part is approximately computed using the simulated path $\{x_{s_q(n)}(t_m), x_{s_q(n)}(t_m+l_1),\ldots, x_{s_q(n)}(t_m+l_{Lq})\}$, i.e.

$$\int_0^{l_{Lq}}\Lambda(x_{s_q(n)}(t_m+\tau), t_m+\tau;\boldsymbol{\theta})\,\mathrm{d}\tau = \sum_{i=1}^{Lq}\Lambda(x_{s_q(n)}(t_m+l_i), t_m+l_i;\boldsymbol{\theta})\Delta l_i. \tag{34}$$

(6) The mean probability density of $\widetilde{x}_{s_q}$ at l_{Lq} is taken as the PDF calculation result of l_{Lq} and the expression is as follows:

$$\hat{f}(l_{Lq}|x_m) \cong \begin{cases} \frac{\sum_{n=1}^{Nq} p_n(l=l_{Lq})}{Nq}, & Nq > 1 \\ p_{Nq}(l=l_{Lq}), & Nq = 1 \end{cases}. \tag{35}$$

The complete RUL PDF curve is obtained by integrating the probability densities of $\{l_{L1}, l_{L2}, \ldots, l_{LQ}\}$.

3. Experiment

3.1. Case 1: experiment on C-MAPSS dataset

To validate the effectiveness of the proposed model, the NASA commercial modular aero-propulsion system simulation (C-MAPSS) turbofan engine dataset is used in this case for RUL prediction [50]. This dataset consists of four subsets (FD001,…, FD004), each of which has different engine operating conditions and failure modes. The subset FD001 with single operating condition and failure mode is selected as the experimental dataset. It contains 26-dimensional data of 100 engines, including the engine number, operating cycle, three operating conditions and monitoring data of 21 sensors. Figure 4 shows the raw data from the sensors used to construct the health indicator (HI).

Since a single sensor has a limited reflection on the system degradation, a weighted fusion method is used to obtain a comprehensive HI [51]. For modeling convenience, the HI should be monotonically varying and has small volatility. Meanwhile, the data differences of HIs at the failure time should be reduced to avoid large uncertainty of the FT. Considering the above factors, the fusion weight of each sensor can be obtained by optimizing the objective function as follows:

$$\widehat{\boldsymbol{\omega}} = \arg\max_{\boldsymbol{\omega}} \frac{1}{4}\left[\sum_{n=1}^{N}\left(\frac{\mathrm{corr}(\boldsymbol{H}_n)}{N} + \frac{\mathrm{mon}(\boldsymbol{H}_n)}{N} + \frac{\mathrm{rob}(\boldsymbol{H}_n)}{N}\right) + \mathrm{con}(\boldsymbol{H}_1, \ldots, \boldsymbol{H}_N)\right], \tag{36}$$

where $\boldsymbol{\omega} = [\omega_1, \ldots, \omega_{Ns}]^{\mathrm{T}}$ and Ns is the number of sensors; $\boldsymbol{H}_n$ is the HI degradation data of the n th specimen; $\mathrm{corr}(\cdot)$, $\mathrm{mon}(\cdot)$, $\mathrm{rob}(\cdot)$, and $\mathrm{con}(\cdot)$ represent the time correlation, monotonicity, robustness, and consistency indicator, respectively, which are used to measure the quality of HI.

Figure 5 shows the HI trajectories of the 30 engine specimens in FD001. Because the values of each specimen at the failure time are different, the RFT is adopted. By introducing state-dependent and time-varying terms into the power function model, the following age- and state-dependent WPM is established as the degradation model:

$$x(t) = x_m + \alpha\int_{t_m}^{t}\left(a x(\tau) + b\tau^{b-1}\right)\mathrm{d}\tau + \beta\int_{t_m}^{t}\sqrt{c\tau + d}\,\mathrm{d}B(\tau), \tag{37}$$

where α and β are the unit-to-unit variability parameters; $\boldsymbol{\theta} = [a, b, c, d]^{\mathrm{T}}$ are the fixed parameters.

The model parameters are estimated according to the method mentioned in section 3. To assess the performance of the IABC algorithm, the commonly used Nelder–Mead algorithm is also introduced for comparison. The initial parameter value ranges for these two methods are consistent. The log-likelihood functions and computation times of 100 estimation experiments are shown in figure 6. From the experimental results, the average estimation results and required time of the IABC algorithm are better than those of the Nelder–Mead algorithm, which indicates that the IABC algorithm is more stable and performs better. By contrast, the Nelder–Mead algorithm is more likely to fall into a local optimum when the initial values are not chosen appropriately.

According to the FTs of the training specimens, the RFT is set to $TN(3.76, 0.012)$ for RUL estimation. One of the remaining engines from FD001 is randomly selected as the test specimen. As shown in figure 7, with the updating of α and β, the predicted RUL is getting closer to the actual RUL. These results illustrate the effectiveness of the parameter update and RUL estimation methods proposed in this paper.

Subsequently, to verify the performance of the proposed model and method, models with improved diffusion terms are selected for comparison [19, 29, 52]. The three types of models, namely M1, M2, and M3, are shown below:

$$\begin{cases} x(t) = x_m + \mu\int_{t_m}^{t} a\tau^{a-1}\mathrm{d}\tau + \int_{t_m}^{t} b\mathrm{d}B(\tau^c) & \text{M1}, \\ x(t) = x_m + \mu\int_{t_m}^{t} a\tau^{a-1}\mathrm{d}\tau + \int_{t_m}^{t}\sqrt{b\mu}\mathrm{d}B(\tau) & \text{M2}, \\ x(t) = x_m + \mu\int_{t_m}^{t} x(\tau)^a\mathrm{d}\tau + \int_{t_m}^{t}\sqrt{b + c\tau}\mathrm{d}B(\tau) & \text{M3} \end{cases}. \tag{38}$$

Note that, μ denotes a random variable that follows a normal distribution in M1 and M2. M1, M2, and M3 use the Bayesian method, Kalman filter, and particle filter, respectively, to update the model. First, to analyze the performance of the different models, the Akaike information criterion (AIC) evaluation index is introduced. As shown in table 1, the AIC of the proposed model for the C-MAPSS dataset is smaller than those of the other models, which indicates that the proposed model has a better fitting performance (the smaller the AIC, the better the model performance).

To further verify the superiority of the proposed method, three engines, S1, S2, and S3, with distinctly different degradation rates (S1 >S2 >S3) are selected as test specimens. Figure 8 shows the RUL PDFs of S1, S2, and S3 at 3/4 lifecycle, and figure 9 gives the mean prediction results of RUL. It can be seen from these two figures that the proposed model performs better in specimens with different degradation rates, which can take into account both higher accuracy and less randomness. In addition, the total mean square error (TMSE) is introduced to evaluate the prediction accuracy of different methods. The smaller the TMSE, the higher the accuracy of the prediction model. As shown in table 2, the TMSEs of the proposed model are the smallest, which indicates the prediction results are more accurate.

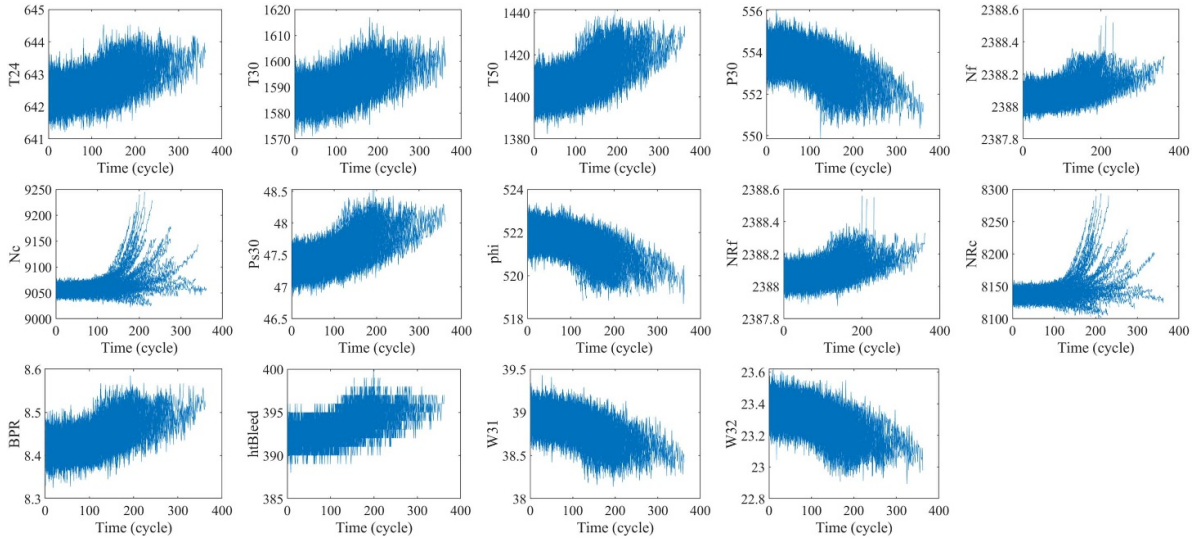

Figure 4. Raw data of the sensors in FD001.

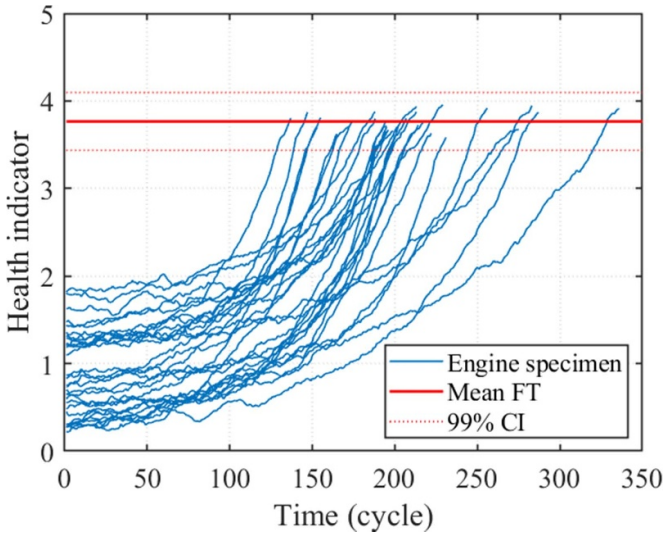

Figure 5. HIs of the 30 C-MAPSS turbofan engines in FD001.

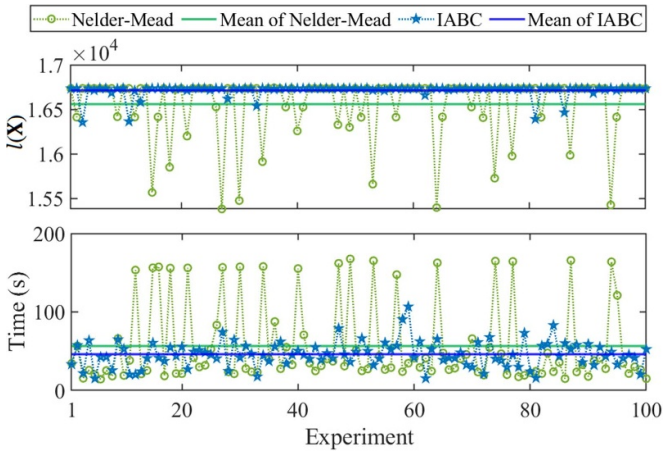

Figure 6. Parameter estimation experiment results of the engine specimens.

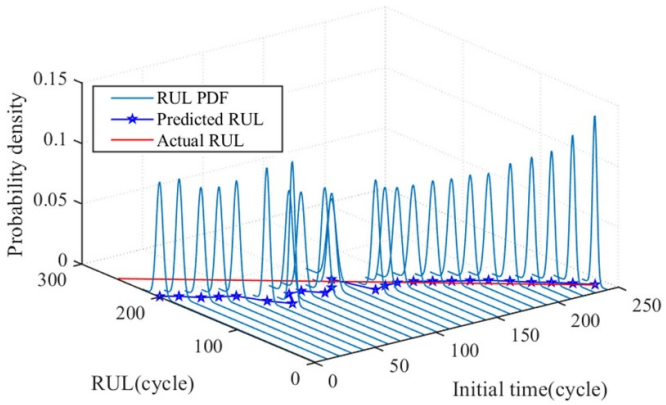

Figure 7. RUL PDFs of the test specimen at different initial times.

Table 1. AICs of different models.

Dataset	M1	M2	M3	Proposed model
C-MAPSS	-3.30×10^4	-3.26×10^4	-3.29×10^4	-3.33×10^4
XJTU-SY	-2.66×10^3	-2.66×10^3	-2.60×10^3	-2.82×10^3

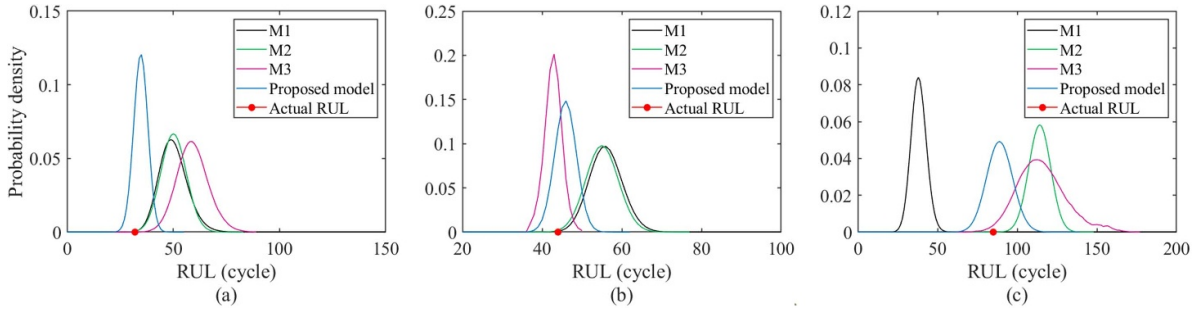

Figure 8. RUL PDFs of the three test engine specimens at 3/4 life-cycle: (a) S1; (b) S2; (c) S3.

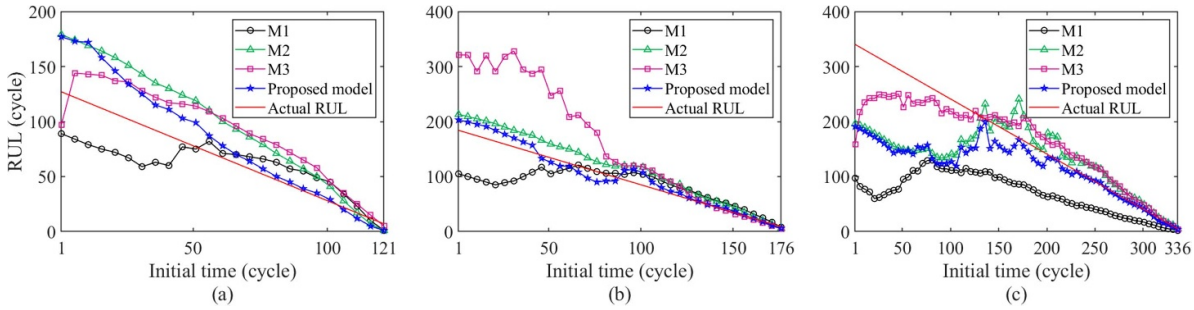

Figure 9. Mean RUL prediction results of the different models for three test engine specimens: (a) S1; (b) S2; (c) S3.

3.2. Case 2: Experiment on XJTU-SY bearing dataset

The XJTU-SY bearing dataset [53] is also used in this section to further validate the effectiveness of the proposed method. The dataset contains the horizontal and vertical vibration signals of 15 bearings under three different working conditions. Five bearings at the speed of 2250 r min^{-1} and the radial force of 11 kN are selected as the experimental subjects. Figure 10 shows the raw signals of five experimental bearings. The FT is set to 25 g. Since the vibration signal cannot directly reflect the bearing degradation, indicators such as peak, root mean square, and frequency domain average amplitude are extracted to construct a new comprehensive HI by using the weighted fusion method introduced in Case 1. The HIs of the bearing specimens from the beginning of degradation are plotted in figure 11.

Table 2. TMSEs of different models for the engine specimens.

Specimen	M1	M2	M3	Proposed model
S1	4.01×10^3	1.33×10^3	1.57×10^3	6.59×10^2
S2	9.28×10^3	5.49×10^2	2.85×10^5	1.73×10^2
S3	6.30×10^4	6.40×10^3	7.13×10^3	6.27×10^3

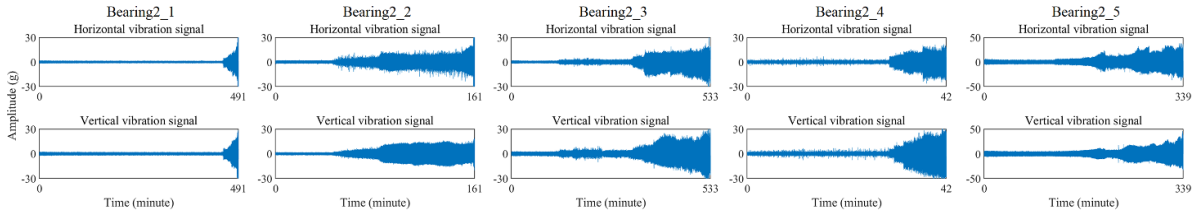

Figure 10. Raw signals of the five experimental bearings.

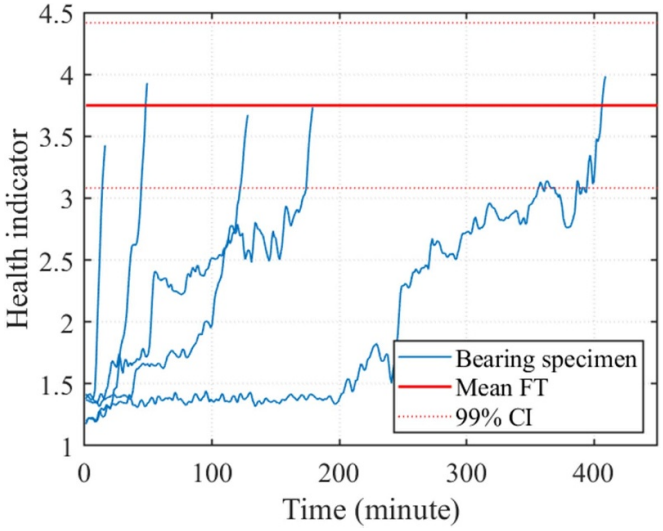

Figure 11. HIs of the five bearing specimens.

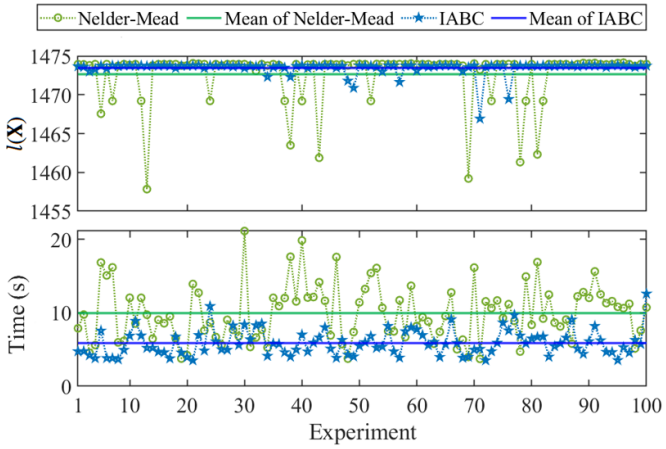

Figure 12. Parameter estimation experiment results of the bearing specimens.

Equation (37) is used as the degradation model. Figure 12 shows experimental results of parameter estimation for the bearing specimens. As can be seen from figure 12, for the bearing dataset, the average estimation results and calculation time of the IABC algorithm are still better than those of the Nelder–Mead algorithm. In addition, it can be seen from table 1 that the AIC of the proposed model is the smallest, which indicates that it has the best performance.

Subsequently, as in Case 1, three test specimens are selected to validate the prediction effect of the proposed method. The RUL PDFs of the three test specimens at 3/4 life-cycle and the mean RUL prediction results of the different models are revealed in figures 13 and 14, respectively. Combining figures 13 and 14, it can be observed that the proposed model has a better prediction effect. Moreover, the TMSEs of the proposed model in the test specimens are also the smallest, as shown in table 3. In conclusion, the prediction model and method proposed in this paper exhibit better performance.

4. Conclusion

An improved age- and state-dependent WPM is proposed in this paper for RUL prediction. The general expression of this model is first established by introducing the time-varying diffusion coefficient with unit-to-unit variability. Then, the IABC algorithm combined with the MLE is introduced for the multi-parameter estimation of the complex degradation model. For parameter updating, an AKF-based method is proposed to update the unit-to-unit variability parameters. In addition, for RUL prediction under the RFT, the analytical expression of the RUL PDF is first derived, and then, the PDF is approximately calculated by the DPS method. Finally, to verify the proposed prediction model and method, the C-MAPSS turbofan

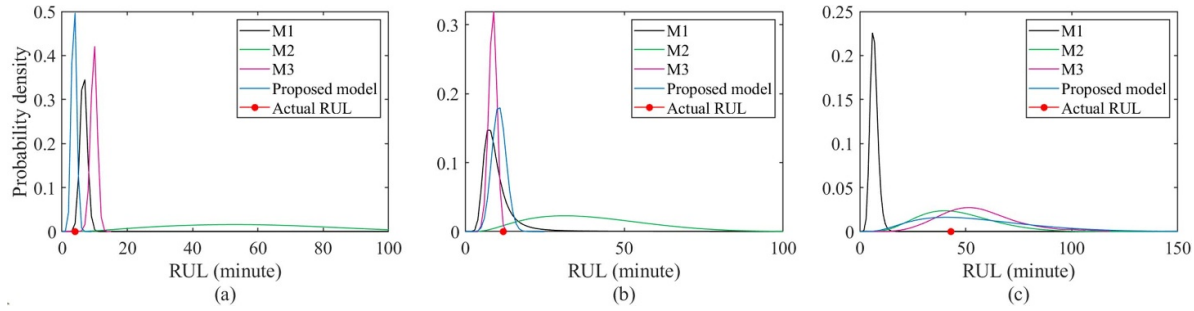

Figure 13. RUL PDFs of the three test bearing specimens at 3/4 life-cycle: (a) S1; (b) S2; (c) S3.

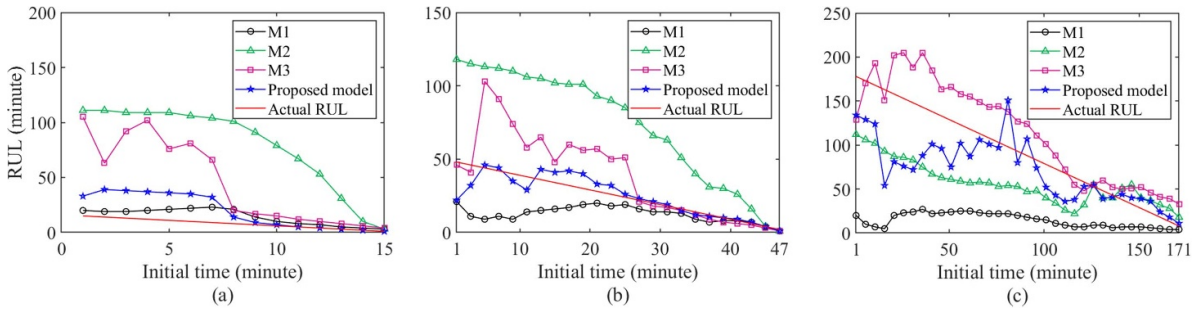

Figure 14. Mean RUL prediction results of the different models for three test bearing specimens: (a) S1; (b) S2; (c) S3.

Table 3. TMSEs of different models for the bearing specimens.

Specimen	M1	M2	M3	Proposed model
S1	1.70×10^3	7.31×10^3	1.70×10^4	1.14×10^3
S2	1.68×10^3	3.61×10^3	1.14×10^3	98.14
S3	2.21×10^4	2.52×10^3	1.46×10^4	2.31×10^3

engine dataset and XJTU-SY bearing dataset are used in the experiment. The results represent that the proposed prediction model and method have better performance.

Data availability statement

The C-MAPSS data that support the findings of this study are openly available at NASA's Open Data Portal: https://data.nasa.gov/Aeorspace/CMAPSS-Jet-Engine-Simulated-Data/ff5v-kuh6, and the XJTU-SY bearing data that support the findings of this study are openly available at Google Drive: https://drive.google.com/open?id=1_ycmG46PARiykt82ShfnFfyQsaXv3_VK.

Acknowledgment

The author acknowledges the support by the Natural Science Foundation of Shanghai Municipality (No. 20ZR1414400) and the Research Projects of CNPC (No. 2022DJ4507).

ORCID iDs

Haoyan Gu https://orcid.org/0009-0002-3731-1569
Yong Li https://orcid.org/0000-0001-7544-2792
Long Jiang https://orcid.org/0000-0001-8082-0719
Zhi Luo https://orcid.org/0000-0001-9909-6900

References

[1] Si X S, Wang W, Chen M Y, Hu C H and Zhou D H 2013 A degradation path-dependent approach for remaining useful life estimation with an exact and closed-form solution *Eur. J. Oper. Res.* **226** 53–66
[2] Zio E 2022 Prognostics and health management (PHM): where are we and where do we (need to) go in theory and practice *Reliab. Eng. Syst. Saf.* **218** 108119
[3] Tsui K L, Chen N, Zhou Q, Hai Y and Wang W 2015 Prognostics and health management: a review on data driven approaches *Math. Probl. Eng.* **2015** 793161
[4] Li K S, Wang R Z, Yuan G J, Zhu S P, Zhang X C, Tu S T and Miura H 2021 A crystal plasticity-based approach for creep-fatigue life prediction and damage evaluation in a nickel-based superalloy *Int. J. Fatigue* **143** 106031
[5] Gu H H, Wang R Z, Tang M J, Zhang X C and Tu S T 2023 Creep-fatigue reliability assessment for high-temperature components fusing on-line monitoring data and physics-of-failure by engineering damage mechanics approach *Int. J. Fatigue* 169 17481
[6] Compare M and Zio E 2025 Opportunities and risks of artificial intelligence for industry 5.0 in the context of reliability and maintenance engineering *J. Reliab. Sci. Eng.* **1** 015001

[7] Peng W, Ye Z S and Chen N 2019 Bayesian deep-learning-based health prognostics toward prognostics uncertainty *IEEE Trans. Ind. Electron.* **67** 2283–93

[8] Chen C, Lu N, Jiang B, Xing Y and Zhu Z H 2021 Prediction interval estimation of aeroengine remaining useful life based on bidirectional long short-term memory network *IEEE Trans. Instrum. Meas.* **70** 1–13

[9] Liu H, Liu Z, Zhang D, Jia W, Xin X and Tan J 2023 Uncertainty quantification and interval prediction of equipment remaining useful life based on semisupervised learning *IEEE Trans. Instrum. Meas.* **73** 1–15

[10] Zezhou W, Jian H, Jiantai Z, Liyuan W and Zhongyi C 2024 Stochastic degradation modeling and remaining useful lifetime prediction based on long short-term memory network *Measurement* **234** 114803

[11] Zhang Z, Si X, Hu C and Lei Y 2018 Degradation data analysis and remaining useful life estimation: a review on Wiener-process-based methods *Eur. J. Oper. Res.* **271** 775–96

[12] Liu D, Wang S and Zhang C 2022 Reliability estimation from two types of accelerated testing data based on an artificial neural network supported Wiener process *Appl. Math. Comput.* **417** 126757

[13] Yang C, Gu X and Xiao Z 2024 Reliability estimation from two types of accelerated testing considering individual difference and measurement error *Probab. Eng. Mech.* **75** 103584

[14] Zhang S, Zhai Q, Shi X and Liu X 2022 A Wiener process model with dynamic covariate for degradation modeling and remaining useful life prediction *IEEE Trans. Reliab.* **72** 214–23

[15] Jia G and Gardoni P 2018 State-dependent stochastic models: a general stochastic framework for modeling deteriorating engineering systems considering multiple deterioration processes and their interactions *Struct. Saf.* **72** 99–110

[16] Pang Z, Si X, Hu C and Zhang Z 2022 An age-dependent and state-dependent adaptive prognostic approach for hidden nonlinear degrading system *IEEE/CAA J. Autom. Sin.* **9** 907–21

[17] Ma Z, Zhao M, Dai X and Chen Y 2023 A hybrid-driven probabilistic state space model for tool wear monitoring *Mech. Syst. Signal Process.* **200** 110599

[18] Zhang Z X, Si X S and Hu C H 2015 An age- and state-dependent nonlinear prognostic model for degrading systems *IEEE Trans. Reliab.* **64** 1214–28

[19] Li N, Lei Y, Guo L, Yan T and Lin J 2017 Remaining useful life prediction based on a general expression of stochastic process models *IEEE Trans. Ind. Electron.* **64** 5709–18

[20] Li N, Lei Y, Yan T, Li N and Han T 2019 A Wiener-process-model-based method for remaining useful life prediction considering unit-to-unit variability *IEEE Trans. Ind. Electron.* **66** 2092–101

[21] Pang Z, Li T, Pei H and Si X 2023 A condition-based prognostic approach for age-and state-dependent partially observable nonlinear degrading system *Reliab. Eng. Syst. Saf.* **230** 108854

[22] Zhai Q, Xu A, Yang J and Zhou Y 2023 Statistical modeling and reliability analysis for degradation processes indexed by two scales *IEEE Trans. Ind. Inform.* **20** 3675–84

[23] He R, König F, Wang Y, Wirsing F, Tian Z, Zuo M and Ye Z 2025 Wear and life predictions for bearings considering simulation-to-reality variability *Mech. Syst. Signal Process.* **229** 112498

[24] Ye Z S, Chen N and Shen Y 2015 A new class of Wiener process models for degradation analysis *Reliab. Eng. Syst. Saf.* **139** 58–67

[25] Wang H, Ma X and Zhao Y 2019 An improved Wiener process model with adaptive drift and diffusion for online remaining useful life prediction *Mech. Syst. Signal Process.* **127** 370–87

[26] Wang Z, Chen Z, Xia T and Pan E 2024 Degradation modeling considering the dependency of rate and volatility for real-time prognostics with error correction *IEEE Trans. Instrum. Meas.* **73** 1–12

[27] Zhang H, Zhou D, Chen M and Xi X 2019 Predicting remaining useful life based on a generalized degradation with fractional Brownian motion *Mech. Syst. Signal Process.* **115** 736–52

[28] Ge R, Zhai Q, Wang H and Huang Y 2022 Wiener degradation models with scale-mixture normal distributed measurement errors for RUL prediction *Mech. Syst. Signal Process.* **173** 109029

[29] Zhou S, Tang Y and Xu A 2021 A generalized Wiener process with dependent degradation rate and volatility and time-varying mean-to-variance ratio *Reliab. Eng. Syst. Saf.* **216** 107895

[30] Li J, Wang Z, Liu X and Feng Z 2023 Remaining useful life prediction of rolling bearings using GRU-DeepAR with adaptive failure threshold *Sensors* **23** 1144

[31] Pan G, Ding X, Li D, Li Y and Wang Y 2023 A reliability evaluation method of complex electromechanical products based on the multi-stress coupling acceleration model *Eng. Fail. Anal.* **146** 107115

[32] Li T, He S and Zhao X 2022 Optimal warranty policy design for deteriorating products with random failure threshold *Reliab. Eng. Syst. Saf.* **218** 108142

[33] Wang Y, Chen X, Zhang S, Fan Z, Hu J and Yang C 2025 A review of modelling and data analysis methods for accelerated test *J. Reliab. Sci. Eng.* **1** 012002

[34] Tang S, Yu C, Feng Y, Xie J, Gao Q and Si X 2016 Remaining useful life estimation based on Wiener degradation processes with random failure threshold *J. Cent South Univ.* **23** 2230–41

[35] Wang Z, Chen Y, Cai Z, Gao Y and Wang L 2020 Methods for predicting the remaining useful life of equipment in consideration of the random failure threshold *J. Syst. Eng. Electron.* **31** 415–31

[36] Wang F, Tang S, Li L, Sun X, Yu C and Si X 2023 Remaining useful life prediction of aero-engines based on random-coefficient regression model considering random failure threshold *J. Syst. Eng. Electron.* **34** 530–42

[37] Wang H, Liao H and Ma X 2021 Remaining useful life prediction considering joint dependency of degradation rate and variation on time-varying operating conditions *IEEE Trans. Reliab.* **70** 761–74

[38] Huang Z, Xu Z, Wang W and Sun Y 2015 Remaining useful life prediction for a nonlinear heterogeneous Wiener process model with an adaptive drift *IEEE Trans. Reliab.* **64** 687–700

[39] Peng C Y and Tseng S T 2009 Mis-specification analysis of linear degradation models *IEEE Trans. Reliab.* **58** 444–55

[40] Si X S, Wang W, Hu C H, Zhou D H and Pecht M G 2012 Remaining useful life estimation based on a nonlinear diffusion degradation process *IEEE Trans. Reliab.* **61** 50–67

[41] Zitouni F and Harous S 2023 Integrating the opposition Nelder–Mead algorithm into the selection phase of the genetic algorithm for enhanced optimization *Appl. Syst. Innov.* **6** 80
[42] Paris P and Erdogan F 1963 A critical analysis of crack propagation laws *J. Fluids Eng.* **85** 528–33
[43] Karaboga D 2005 An idea based on honey bee swarm for numerical optimization *Technical report-tr06*
[44] Gao W and Liu S 2011 Improved artificial bee colony algorithm for global optimization *Inf. Process. Lett.* **111** 871–82
[45] Ghambari S and Rahati A 2018 An improved artificial bee colony algorithm and its application to reliability optimization problems *Appl. Soft Comput.* **62** 736–67
[46] Zhang S J, Kang R and Lin Y H 2021 Remaining useful life prediction for degradation with recovery phenomenon based on uncertain process *Reliab. Eng. Syst. Saf.* **208** 107440
[47] Bi H, Ma J and Wang F 2015 An improved particle filter algorithm based on ensemble Kalman filter and Markov chain Monte Carlo method *IEEE J. Sel. Top. Appl. Earth Obs. Remote Sens.* **8** 447–59
[48] Fraser C T and Ulrich S 2021 Adaptive extended Kalman filtering strategies for spacecraft formation relative navigation *Acta Astronaut.* **178** 700–21
[49] Zio E and Compare M 2013 Evaluating maintenance policies by quantitative modeling and analysis *Reliab. Eng. Syst. Saf.* **109** 53–65
[50] Si X and Ren Z 2019 A data-fusion based prognostic method for complex degrading system *2019 Prognostics and System Health Management Conf.* (PHM–Qingdao)
[51] Gu L, Zheng R, Zhou Y, Zhang Z and Zhao K 2022 Remaining useful life prediction using composite health index and hybrid LSTM-SVR model *Qual. Reliab. Eng. Int.* **38** 3559–78
[52] Wang X, Balakrishnan N and Guo B 2014 Residual life estimation based on a generalized Wiener degradation process *Reliab. Eng. Syst. Saf.* **124** 13–23
[53] Wang B, Lei Y, Li N and Li N 2020 A hybrid prognostics approach for estimating remaining useful life of rolling element bearings *IEEE Trans. Reliab.* **69** 401–12

Haoyan Gu received the MS degree in mechanical engineering at East China University of Science and Technology, Shanghai, China, in 2024. His research interests include fault diagnosis and data-driven remaining useful life prediction.

Yong Li, PhD, Associate Professor, received the PhD degree in instrument science and technology from Xi'an Jiaotong University, Xi'an, China, in 2014. He is currently an Associate Professor at the School of Mechanical and Power Engineering, East China University of Science and Technology, Shanghai, China. His research interests include non-stationary nonlinear signal processing, health monitoring and fault diagnosis for rotating machinery.

Long Jiang, PhD, senior engineer, is the director of New Energy Center, National Key Laboratory of Oil and Gas Drilling and Production and Transportation Equipment, Engineering Materials Research Institute of China Petroleum Group Co. Ltd He is mainly engaged in the research and development of new energy, oil and gas drilling and transportation equipment.

Zhi Luo received the PhD degree in mechatronic engineering from Xi'an Jiaotong University, Xi'an, China, in 2020. He is currently a Lecturer at the School of Mechanical and Power Engineering, East China University of Science and Technology, Shanghai, China. His research interests include structural health monitoring, and nondestructive testing for metal and composite materials based on guided wave detection methods.